PCCP

Accepted Manuscript

ROYAL SOCIETY OF CHEMISTRY

www.rsc.org/pccp

Clay-Supported Novel Bimetallic Core–Shell Co□Pt and Ni□Pt Nanocrystals with High Catalytic Activities

Dharmesh Varade[2,3] and Kazutoshi Haraguchi[1,2]*

1. Dep. of Applied Molecular Chemistry, College of Industrial Technology, Nihon University, 1-2-1 Izumi-cho, Narashino, Chiba 275-8575, Japan
2. Material Chemistry Laboratory, Kawamura Institute of Chemical Research, 631 Sakado, Sakura, Chiba 285-0078, Japan
3. Dep. of Chemical Engineering, Institute of Engineering & Technology, Ahmedabad University, Nr. Commerce Six Roads, Navrangpura, Ahmedabad-380 009, Gujarat, India

*Corresponding Author

E-mail: haraguchi.kazutoshi@nihon-u.ac.jp

We demonstrate the striking potential of exfoliated clay (synthetic hectorite; Laponite XLG) platelets to prepare bimetallic (Co–Pt and Ni–Pt) NCs with well-defined structures. Catalytic studies show a strong bimetallic synergistic effect of the core–shell NCs; their catalytic activities are much higher than those of monometallic NCs and other bimetallic core–shell NCs.

Bimetallic core–shell nanocrystals (NCs) with controlled size, shape, and structure are emerging as highly important materials with attractive potential for effective tuning of their catalytic properties.[1-3] Among core–shell NCs of various combinations, those comprising an inexpensive metal core and a noble metal shell have received particular interest because of the functional and economic advantages that they provide.[4-10]

Pt-based NCs have long been used as catalytic materials, especially for energy applications such as fuel cells.[11] Alloying Pt with other nonprecious metals has proven to be an efficient approach to improve the catalytic activity, enhance resistance to CO poisoning, and lower the cost.[12-17] A large variety of such bimetallic NCs are available, including Pt/Ni,[4,13] Pt/Fe,[13,15] Pt/Co,[13,16,17] Pt/Ru,[14] with a wide range of applications. Particularly, Pt/Co and Pt/Ni NCs show alluring multifunctional behavior such as good electrical, catalytic, and magnetic properties, together with high stability.[13,16,17] However, the simple and direct method for the creation of well-defined bimetallic core–shell Co–Pt and Ni–Pt NCs has seen limited success and is still a challenge for the development of multifunctional smart materials.[1] Moreover, it is fairly difficult to obtain core–shell NCs smaller than 20 nm, especially in the absence of a surfactant.

Considering the limitations of previous syntheses in controlling the size and composition of Co–Pt and Ni–Pt NCs, the effective synthesis of these highly relevant bimetallic NCs with

precise control of the particle size and morphology is of importance. Recently we found that ascribed to the unique interaction of the clay platelets with a variety of metal ions,[18,19] it plays a crucial role in the creation and stabilization of nanocrystals and impart them high stability and a large BET surface area.[18,20-22] Inspired by this conception, we have prepared Pt-based bimetallic core–shell Co–Pt and Ni–Pt NCs in the presence of clay (synthetic hectorite; Laponite XLG). The structure of the clay is stable up to 500 ^{0}C. The resulting small bimetallic NCs with well-defined shapes can provide more Pt active sites and a larger surface area, which makes these materials highly promising catalysts. Moreover, this synthesis affords an expedient and environmentally benevolent route to large-scale production because it does not require high temperatures, organic additives, or electrochemical deposition.

In this study, the Pt-based bimetallic core–shell NCs, namely, Co–Pt, and Ni–Pt NCs, were prepared in a single step using a facile wet-chemical co-reduction method. First, a stable aqueous dispersion of exfoliated clay platelets (Laponite XLG: 2 wt %) was prepared; the dispersion was homogeneous, nearly transparent, and had a fairly high pH (10.2) and zeta potential (–37.1 mV) as a result of the negatively charged two-dimensional silicate nanosheets. In a typical synthesis of Co–Pt bimetallic NCs (Pt/Co molar ratio = 1.0), K_2PtCl_4 solution (10 mL; 20 mM) and $CoSO_4 \cdot 7H_2O$ solution (10 mL; 20 mM) were mixed with a clay dispersion (10 mL; 2 wt%) in a vial to give a homogeneous mixture (**Scheme S1** in the Supporting Information). The precursor ions interacted with the clay platelets upon mixing, and the subsequent addition of a freshly prepared aqueous solution of $NaBH_4$ (10 mL; 0.2 M) induced the co-reduction of the metal ions in the presence of clay. The vial

was capped and left under static conditions for 24 h to enable the formation of bimetallic NCs.

The resulting products were collected by washing/centrifugation cycles with water. For further characterization, the product was redispersed in water to produce a stable colloidal suspension. A similar method was used to prepare the Ni–Pt NCs. In contrast, when the above synthesis was performed in the absence of clay under otherwise identical synthetic conditions, rigorous particle aggregation was observed as precipitates in both systems (**Figure S1**), explicitly demonstrating that clay played a key role as a competent stabilizer and also a structure-directing agent in the creation of the bimetallic NCs. In brief, exfoliated clay platelets with charged surfaces interact with precursor ions. Then, the controlled reduction of metal ions near the clay surface was occurred by addition of $NaBH_4$, in which the clay induces the spontaneous separation of the deposited Ni(Co) and Pt, and preventing their random growth resulting in the one-pot formation of Ni(Co)–Pt core–shell NCs. Here, the metal composition of Co or Ni is 50 atom % in the bimetallic Pt-NCs.

A representative low-magnification transmission electron microscopy (TEM) image of the as-prepared Co–Pt NCs, presented in **Figure 1a**, illustrates the successful formation of uniform and spherical bimetallic Co–Pt NCs *ca*. 15–18 nm in size with a well-defined morphology. The thickness of Pt-shell is estimated 3.0–3.5 nm from the composition. The magnified TEM image for a single NC is shown as the inset in Figure 1a. The high-resolution TEM (HRTEM) image depicts that these NCs are highly crystalline with well-defined fringes; the periodicity of the lattice is approximately 0.21 nm for Pt in the shell region (**Figure 1b**). The high-angle annular dark-field scanning TEM (HAADF-STEM) image in **Figure 1c** shows a clear contrast between the core and the shell in the Co–Pt

structural morphology; the darker core (Co) coated by a brighter shell (Pt) in each particle is ideal, validating this technique as a direct and feasible way of creating small and well-defined core–shell hybrid nanostructures with a high content and good dispersion of metals. The corresponding selected-area electron diffraction (SAED) patterns in **Figure 1d** exhibit ring arrays with intense spots assigned to the (111), (200), (220), and (311) planes of face-centered cubic (*fcc*) Pt crystals in the shell region. An energy dispersive X-ray spectroscopy (EDX) analysis of the NCs (**Figures 1e** and **1f**) confirms the presence of Co and Pt with a Co-rich core and a Pt-rich shell, thus verifying the formation of bimetallic Co–Pt core–shell NCs.

Distinct bimetallic core–shell-type Co–Pt NCs are formed through the use of clay platelets, via controlled nucleation and metal cluster formation without agglomeration. Concerning the co-reduction, because Co and Pt ions have very different reduction potentials (Co = –0.29 eV and Pt = +0.76 eV),[23,24] the reduction of Co ions occurs preferentially over that of Pt ions. In fact, under the same reduction conditions using individual ions and clay, the Co ions reduced in a short time (within 2–3 min), while the Pt ions required quite a long time to be reduced (15–20 min). Then, in the co-reduction, the reduction of Co ions occurs preferentially to produce Co cores, followed by the overgrowth of Pt NCs on the Co seeds in the presence of clay.

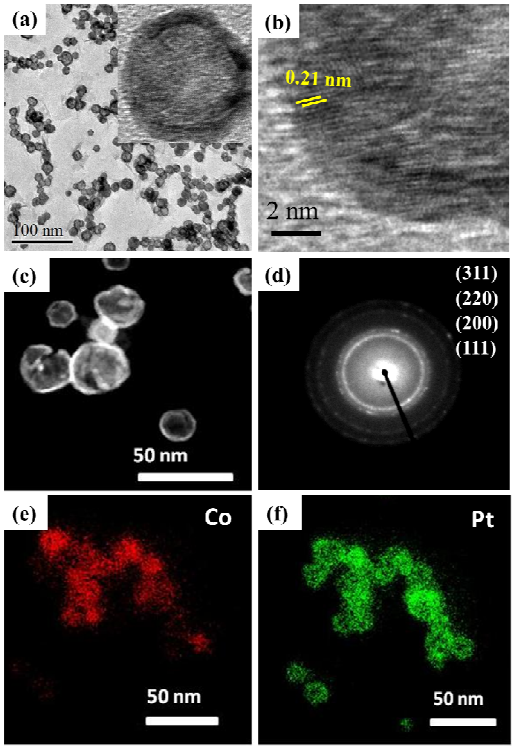

Figure 1: Bimetallic core–shell Co–Pt NCs. (a) Low-magnification transmission electron microscopy (TEM) image. Inset shows the magnified TEM image. (b) High-resolution TEM (HRTEM) image depicting well-defined fringes. (c) High-angle annular dark-field scanning TEM (HAADF-STEM) image. (d) Corresponding selected-area electron diffraction pattern showing ring arrays with intense spots assigned to the (111), (200), (220), and (311) planes of face-centered cubic (*fcc*) Pt crystals. Energy-dispersive X-ray mapping confirms the presence of (e) Co in the core, and (f) Pt in the shell.

By assuming the clay density to be 2.56 g/cm^3 and considering the clay size (30 nm diameter and 1nm thick), the number of clay platelets in the solution was calculated as 2.6 × 10^{15}, which means that there are ~5000 ions each of Co and Pt for every clay platelet. In the solution, both ions (Co and Pt) interact with the exfoliated clay platelet, as revealed by the increase in viscosity (**Figure S2**). This may be caused by the interaction of anionic precursor ions with the clay due to the positively charged clay rims. Thus, the clay may decrease the rate of the movement of the ionic species in the solution. Accordingly, the reduction in the next step (with $NaBH_4$) may be decelerated under these diffusion-limited conditions.[25] The addition of $NaBH_4$ will first induce the controlled reduction of Co ions

near the clay surface. The coalescence of Co atoms leads to the formation of Co clusters, which ultimately grow into definite NCs between the clay platelets that likely adhere to the silicate surface. Subsequently, Pt ions are reduced; the nucleation of Pt atoms may be energetically more favorable on the surface of the Co NCs, resulting in the one-pot formation of the Co–Pt core–shell NCs with an inner Co core and an outer Pt shell. Furthermore, the interaction of these NCs with the clay counteracts the inherent van der Waals attractions among the spherical core–shell NCs, preventing their random growth. In the absence of clay, the co-reduction of Co and Pt ions formed large inhomogeneous aggregates with ill-defined structures (**Figure S1**, inset). Also, with clay, the use of organic components can be circumvented. It is therefore inferred that clay plays a pivotal role in the fabrication of the small bimetallic core–shell Co–Pt NCs, leading to core–shell structures suitable for use in various applications.

Ni–Pt bimetallic NCs (**Figure 2**) were also prepared in a similar manner; these NCs are not easy to prepare using conventional methods.[13] The representative TEM images in **Figure 2a** demonstrate the successful formation of well-defined core–shell Ni–Pt NCs approximately 12–15 nm in size. Figure 2a also depicts a clear contrast between the core and the shell in the Ni–Pt structural morphology. The thickness of Pt-shell is estimated 2.4–3.0 nm from the composition. The corresponding SAED patterns (**Figure 2b**) show ring arrays with intense spots assigned to the (111), (200), (220), and (311) planes of *fcc* Pt crystals in the shell region. **Figure 2c** shows the HAADF-STEM images, while the corresponding EDX mapping is shown in **Figures 2d** and **2e**, confirming the composition and separation of the two elements, i.e., a Ni-rich core and a Pt-rich shell in the Ni–Pt core–shell NCs. This morphology is also caused by the large difference between the reduction

potentials of Ni and Pt ions (Ni = –0.25 eV, Pt = +0.76 eV). The reduction of Ni ions preferentially occurs in a short time period (within 2–3 min) to produce Ni cores, followed by the formation of a Pt shell, in a similar manner to the Co–Pt system.

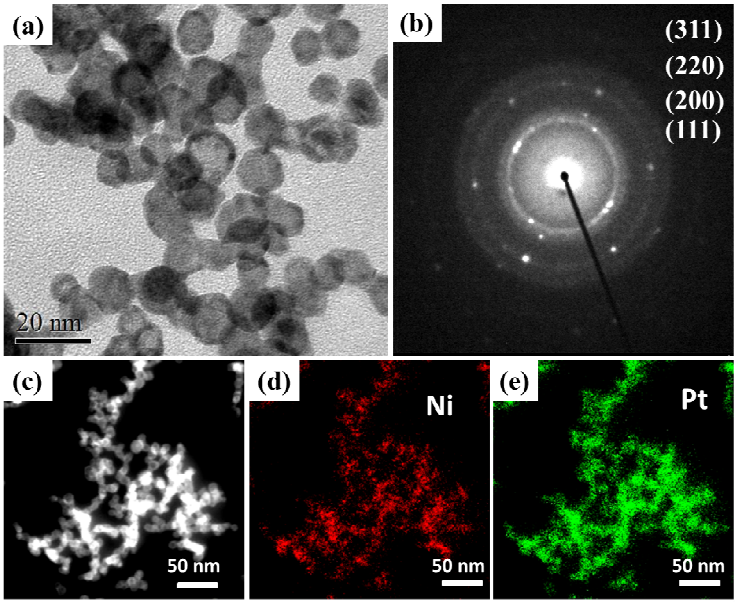

Figure 2: (a) Low-magnification transmission electron microscopy (TEM) image of Ni–Pt core–shell bimetallic NCs. (b) Corresponding SAED patterns showing ring arrays with intense spots assigned to the (111), (200), (220), and (311) planes of *fcc* Pt crystals. (c) HAADF-STEM image and energy-dispersive X-ray spectroscopy (EDX) elemental mappings of (d) Ni and (e) Pt, indicating the formation of Ni–Pt core–shell NCs.

Ni–Pt (Co–Pt) NCs exhibited the crystalline Ni(Co) and Pt peaks in X-ray diffraction pattern (results not shown) which are consistent with the results of HRTEM images and SAED patterns. X-ray photoelectron spectroscopy (XPS) measurements for the bimetallic Co–Pt and Ni–Pt core–shell NCs confirmed the presence of individual metallic Pt, Co, and Ni (**Figure S3**). Also, XPS data reveals the oxide phases of Co (CoO: Binding energy $Co2p_{3/2}$ = 779.7 eV) and Ni (NiO: Binding energy $Ni2p_{3/2}$= 853.7 eV). Furthermore, the inclusion of clay is a promising strategy for improving the specific surface areas of the resulting composite nanomaterials. N_2 adsorption–desorption measurements show that the Co–Pt core–shell NCs (Co–Pt/clay NCs) have high BET surface areas of 240 m^2g^{-1} (**Figure**

S4), although the value is appreciably decreased from that of the clay (314 m^2g^{-1}). On the other hand, the average pore size (4.51 nm) and pore volume (0.14 cm^3g^{-1}) of the composite material depicts minor increase from that of the clay probably owing to the occurrence of these nanocrystals in the interlayers of the clay. This slight increase in the size of the mesopores is clearly reflected by a change in the nature of the isotherm. As-prepared composites fabricated with designed compositions and desired functions, e.g., superior catalytic properties, are therefore expected to be attainable.

The novel Co–Pt and Ni–Pt core–shell NCs were tested for the reduction of 4-nitrophenol with $NaBH_4$ as a model system to assess their catalytic activities (**Figure S5a**). The reduction of 4-nitrophenol with $NaBH_4$ did not progress in the absence of a catalyst; the absorption intensity of 4-nitrophenol remained unaltered even after 90 min (**Figure S5b**). In the presence of a very small amount of Co–Pt (**Figure 3(a-1)**) or Ni–Pt (**Figure 3(b-1)**) core–shell NCs, the strong ultraviolet (UV) absorption peak at 400 nm rapidly diminished (due to the reduction of 4-nitrophenol), demonstrating high catalytic activity. In the reduction process, the overall concentration of $NaBH_4$ was much higher than that of 4-nitrophenol, so pseudo-first-order kinetics could be applied with respect to 4-nitrophenol in order to determine the catalytic activity. As expected, a linear correlation was obtained between $\ln(A_t/A_0)$ and the reduction time, as depicted in **Figure 3(a-2)** and Figure **3(b-2)** (A_t and A_0 represent the absorbance at time t and the initial absorbance of 4-nitrophenolate ions, respectively); the slope provides the rate constant (k). In order to estimate the catalytic performances of the catalysts, the activity parameter $\kappa = k/m$ (the ratio of the rate constant to the total mass of catalyst added) was determined. All these parameters are summarized in **Table 1**. It is worth mentioning that monometallic Co or Ni NCs prepared in the presence

of clay show negligible or almost no catalytic activity for this reaction (data not shown), while monometallic Pt NCs prepared in the presence of clay shows good catalytic activity (**Figure S6**). However, the presence of these non-precious metals (Co and Ni) as a core together with a noble Pt metal as a shell can significantly enhance (more than 100 times) the performance and activity of the Pt catalyst. Moreover, the activity parameter is much higher (240–400 times) when it is evaluated based on the Pt loading (κ per Pt weight) (**Table 1**), which indicates that these bimetallic NCs are more significant from the viewpoint of Pt loading. In the two bimetallic NCs, the Co–Pt core–shell NC was more active (κ = 110) than the Ni–Pt core–shell NC (κ = 63.3), as shown in Figure 3 and **Table 1**. This may be attributed to the homogeneous distribution of elements (as illustrated in **Figure 1e** and **1f**), i.e., the high modulation of the Pt electric properties, in the Co–Pt core–shell NCs. In addition to being more active than monometallic Pt NCs (κ = 0.53, **Table 1**), the catalytic activity of the Co–Pt and Ni–Pt core–shell NCs were significantly higher than those of previously reported Pd–Pt (κ = 1.70) and Au–Pt (κ = 0.53) core–shell NC catalysts,[18] demonstrating the very high value of these materials. These may be ascribed to the modification of the electronic structure[7] due to the presence of Ni or Co, although the nature of the key reaction intermediates, the mechanism, and the active ensemble are still unresolved. In addition, these small core–shell NCs are highly beneficial for use as nanocatalysts, primarily because of their higher stability and resistance to agglomeration as a result of the clay, as shown in **Figure S7**. The high catalytic activities observed in the present study can also be attributed to the presence of clay, which imparts a well-defined core–shell morphology, size uniformity, high surface area, and stability to the NCs. Moreover, catalysts shows almost similar activity even after 4-5 cycles revealing the

stability of this material. The material shows no change in particle size and shape even after catalytic application. A study of the detailed mechanism of the formation and the use of the materials as electrocatalysts is currently underway.

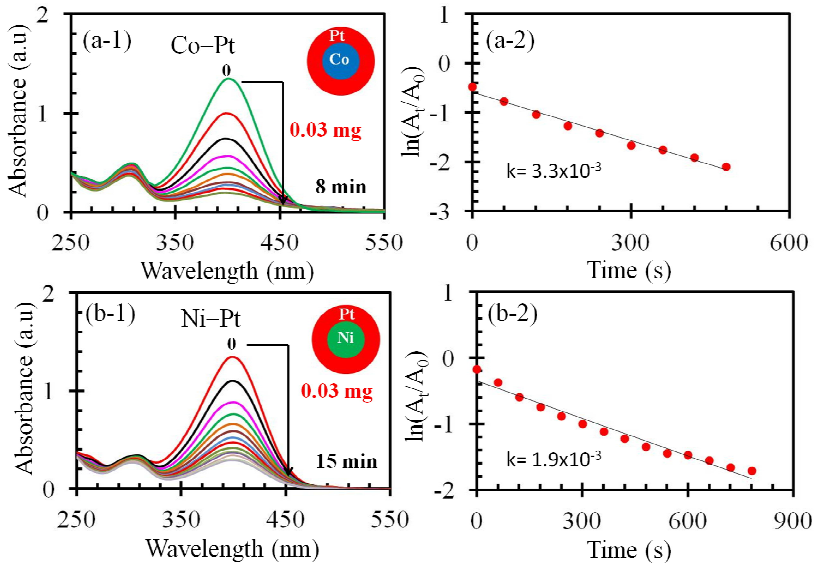

Figure 3: Temporal evolution of UV-vis spectra for the reduction of 4-nitrophenol by $NaBH_4$ in presence of (a-1) Co–Pt and (b-1) Ni–Pt NCs. The insets show the core–shell morphologies of the composites. The corresponding linear correlations of $\ln(A_t/A_0)$ with time is depicted in (a-2) and (b-2), respectively. The black lines show the slopes, which correspond to the rate constants (k).

Table 1: Summary of Amount of Catalysts Used (m), Rate Constant (k), and Activity Parameters (κ).

Catalyst	Weight* m (mg)	Rate Constant k (s^{-1})	Activity Parameter κ ($s^{-1}g^{-1}$)	Activity Parameter per Pt κ ($s^{-1}g^{-1}$)
Co–Pt	0.03	3.3×10^{-3}	110	220
Ni–Pt	0.03	1.9×10^{-3}	63.3	126.6
Pt	3.0	1.6×10^{-3}	0.53	0.53

* The weight is the amount of NCs composite with clay.

CONCLUSIONS

In conclusion, this easy, one-step synthesis in the presence of clay results in the formation of distinct core–shell type bimetallic (Co–Pt and Ni–Pt) NCs. The clay plays a crucial role

in the formation and stabilization of the core–shell assemblies. The resulting Co–Pt and Ni–Pt NCs exhibit extraordinarily high catalytic activities compared with monometallic Pt and previously reported bimetallic Pt catalysts. This is attributed to the well controlled morphology (core–shell), small size (<20 nm), high surface area, and high stability of the NCs. Intriguingly, the presence of clay provides a high stability and a large BET surface area and further improves the catalytic activity of the core–shell NC/clay composites. The results of this study will help develop more rational approaches to superior multifunctional catalysts using clay minerals.

ACKNOWLEDGEMENTS

This work was supported by the Ministry of Education, Science, Sports and Culture of Japan (Grant-in-Aid 23350117). The authors thank DIC Analysis Center (DIC Corp.) for the TEM-EDX and XPS measurements.

REFERENCES

1. Chaudhuri, R. G.; Paria, S. *Chem. Rev.* **2012**, *112*, 2373–2433.
2. Sinfelt, J. H. *Bimetallic Catalysts: Discoveries, Concepts and Applications*; John Wiley and Sons: New York, **1983**.
3. Liu, X.; Liu, X. *Angew. Chem. Int. Ed.* **2012**, *51*, 3311–3313.
4. Wang, S. B.; Zhu, W.; Ke, J.; Gu, J.; Yin, A.; Zhang, Y.; Yan, C. *Chem. Commun.* **2013,** *49*, 7168−7170.
5. Zhou, S.; Varughese, B.; Eichhorn, B.; Jackson, G.; Mcllwrath, K. *Angew. Chem. Int. Ed.* **2005**, *44*, 4539–4543.
6. Wang, D.; Xin, H. L.; Wang, H.; Yu, Y.; Rus, E.; Muller, D. A.; DiSalvo, F. J.; Abruna, H. D. *Chem. Mater.* **2012**, *24*, 2274−2281.
7. Yan, J.; Zhang, X.; Akita, T.; Haruta, M.; Xu, Q. *J. Am. Chem. Soc.*, **2010**, *132*, 5326–5327.
8. Wang, X.; Altmann, L.; Stover, J.; Zielasek, V.; Baumer, M.; Al-Shamery, K.; Borchert, H.; Parisi, J.; Kolny-Olesiak, J. *Chem. Mater.* **2013**, *25*, 1400−1407.
9. Tao, F.; Grass, M. E.; Zhang, Y. W.; Butcher, D. R.; Renzas, J. R.; Liu, Z.; Chung, J. Y.; Mun, B. S.; Salmeron, M.; Somorjai, G. A. *Science* **2008**, *322*, 932–934.
10. Varade, D.; Abe, H.; Yamauchi, Y.; Haraguchi, K. *ACS Appl. Mater. Interfaces* **2013**, *5*, 11613–11617.
11. Chen, A.; Holt-Hindle, P. *Chem. Rev.* **2010,** *110,* 3767–3804.
12. Liu, Z.; Hu, J. E.; Wang, Q.; Gaskell, K.; Frenkel, A. I.; Jackson, G. S.; Eichhorn, B. *J. Am. Chem. Soc.*, **2009**, *131*, 6924–6925.
13. Wang, C.; Chi, M.; Li, D.; van der Vliet, D.; Wang, G.; Lin, Q.; Mitchell, J. F.; More, K. L.; Markovic, N. M.; Stamenkovic, V. R. *ACS Catal.* **2011**, *1*, 1355–1359.
14. Yang, L.; Vukmirovic, M. B.; Su, D.; Sasaki, K.; Herron, J. A.; Mavrikakis, M.; Liao, S.; Adzic, R. R. *J. Phys. Chem. C* **2013**, *117*, 1748−1753.
15. Chen, H.; Wang, D.; Yu, Y.; Newton, K. A.; Muller, D. A.; Abruna, H.; DiSalvo, F. J. *J. Am. Chem. Soc.* **2012**, *134*, 18453−18459.
16. Bigot, J.; Kesserwan, H.; Halté, V.; Ersen, O.; Moldovan, M. S.; Kim, T. H.; Jang, J.; Cheon, J. *Nano Lett*. **2012**, *12*, 1189−1197.
17. Song, C.; Wang, Y.; Rosi, N. L. *Angew. Chem. Int. Ed*. **2013**, *52*, 3993–3995.
18. Varade, D.; Haraguchi, K. *Chem. Commun.,* **2014**, *50*, 3014–3017.
19. Haraguchi, K.; Li, H.; Matsuda, K.; Takehisa, T.; Elliott, E. *Macromolecules* **2005**, *38,* 3482−3490.
20. Varadwaj, G. B. V.; Parida, K. M. *RSC Advances* **2013**, *3*, 13583–13593.
21. Datta, K. K. R.; Eswaramoorthy, M.; Rao, C. N. R. *J. Mater*. Chem. **2007**, *17*, 613–615.
22. Varade, D.; Haraguchi, K. *Langmuir* **2013**, *29*, 1977–1984.
23. Shevchenko, E. V.; Talapin, D. V.; Rogach, A. L.; Kornowski, A.; Haase, M.; Weller, H. *J. Am. Chem. Soc.* **2002**, *124*, 11480−11485.
24. Ataee-Esfahani, H.; Wang, L.; Nemoto, Y.; Yamauchi, Y. *Chem. Mater.* **2010**, *22*, 6310−6318.
25. Papp, S.; Patakfalvi, R.; Dékány, I. *Croat. Chem. Acta* **2007**, *80*, 493−502.